Journal of Catalysis 365 (2018) 411–419

Contents lists available at ScienceDirect

Journal of Catalysis

journal homepage: www.elsevier.com/locate/jcat

Efficient selective oxidation of propylene by dioxygen on mesoporous-silica-nanoparticle-supported nanosized copper

Nien-Chu Lai [a], Ming-Chieh Tsai [a], Chun-Hsia Liu [b], Ching-Shiun Chen [c,d], Chia-Min Yang [a,e,*]

[a] Department of Chemistry, National Tsing Hua University, Hsinchu 30013, Taiwan
[b] National Synchrotron Radiation Research Center, Hsinchu 30076, Taiwan
[c] Center for General Education, Chang Gung University, Taoyuan City 33302, Taiwan
[d] Department of Pathology, Chang Gung Memorial Hospital, Taoyuan City 33302, Taiwan
[e] Frontier Research Center on Fundamental and Applied Sciences of Matters, National Tsing Hua University, Hsinchu 30013, Taiwan

ARTICLE INFO

Article history:
Received 22 April 2018
Revised 25 June 2018
Accepted 4 July 2018

Keywords:
Nanosized copper
Mesoporous silica nanoparticles
Metal dispersion
Selective propylene oxidation
In situ measurement

ABSTRACT

A direct synthetic route was developed to prepare mesoporous-silica-nanoparticle-supported copper catalysts featuring ordered mesostructures with extensive intraparticle voids, a high degree of silica condensation, and a high dispersion of copper species. After hydrogen reduction, the catalysts containing nanosized metallic copper showed superior and stable catalytic activity for the selective oxidation of propylene by dioxygen, with high conversion of both reactants and high yield and formation rate of acrolein. The best catalyst outperformed the state-of-the-art silica-supported copper catalysts, representing one of the most active acrolein-production catalysts. Results of in situ X-ray absorption spectroscopy, in situ diffuse reflectance infrared Fourier transform spectroscopy, and other characterizations suggested that the metallic copper transformed and mainly stayed in the 1+ oxidation state under reaction conditions and that factors including the small size of copper and the presence of silanol groups on the silica support were crucial for the catalytic performance of the catalysts.

1. Introduction

Supported nanocatalysts containing highly dispersed metals generally exhibit high activity in heterogeneous catalysis, mainly owing to their high surface area with an abundance of low-coordination surface sites [1–8]. The preparation of metal nanocatalysts on high-surface-area supports remains challenging because nanosized metals tend to agglomerate or sinter during catalyst preparation and/or under catalytic reactions [1,3,4,6,8]. This is especially true for the preparation of copper catalysts, which have been widely applied in important industrial processes [9,10] and are promising for selective oxidation [11–21], hydrogenation [22–25], photocatalysis [26–29], and other reactions. Methods including ammonia-induced deposition precipitation [6,30], fatty-acid-assisted assembly [31,32], solid state grinding [33,34], vacuum thermal preparation [15], and co-gelation [35] have been reported to deposit copper particles on high-surface-area silicas, but the dispersion of copper remains low for these materials. Obviously, there is a strong need for new strategies to prepare high-surface-area silica-supported nanosized copper catalysts.

Among the reactions catalyzed by copper, the selective oxidation of propylene with dioxygen (O_2) to produce acrolein is of great interest [11,15,17,20,36,37] because it is a green reaction that produces the high-value-added acrolein for the manufacture of acrylic acid, methionine, and other important chemicals [11,38–40]. Supported copper catalysts have been shown to be active for this reaction, with the product selectivity mainly associated with the oxidation state of copper and the reaction temperature [1,11,17,19,20,41]. Supported CuO_x [11,15] and copper-incorporated zeolites [41,42] are reported to produce acrolein, with CO_2 and ethanal as main byproducts, and higher reaction temperatures result in higher propylene conversion accompanied by decreased acrolein selectivity. Making small Cu (or CuO_x) particles on high-surface-area supports has been suggested to be a way of achieving high propylene conversion and high acrolein selectivity simultaneously at relatively low temperature [1,6]. Recently, we reported a method of preparing highly dispersed copper nanoparticles on mesoporous SBA-15 silica [15]. The SBA-15-supported copper catalysts exhibited high conversion of propylene and high selectivity for acrolein and outperformed other silica-supported copper catalysts [43]. The study indicates that the small

* Corresponding author at: Department of Chemistry, National Tsing Hua University, Hsinchu 30013, Taiwan.
E-mail address: cmyang@mx.nthu.edu.tw (C.-M. Yang).

https://doi.org/10.1016/j.jcat.2018.07.014
0021-9517/

size of copper is the most crucial factor in high catalytic activity for the reaction. In addition to the size effect, the surface properties of the support may also affect the catalytic performance of the supported catalysts. For example, Fukuoka et al. found a promotional effect of the surface silanol groups in the preferential oxidation of carbon monoxide catalyzed by platinum nanoparticles supported on mesoporous FSM-16 silica [44]. Nevertheless, for supported copper catalysts, the possible influence of the surface properties of the support on their catalytic performance has seldom been discovered and studied.

Here we report a direct synthesis of MCM-41-type mesoporous silica nanoparticle (MSN)-supported nanosized copper catalysts and catalytic studies on the selective oxidation of propylene with O_2. The synthesis was based on the "pH-jump" synthesis of mesoporous MCM-41 silica [45], with the ammonia complex of Cu(II) as the metal precursor. The addition of ethyl acetate (EA) caused a drastic drop in solution pH and simultaneously initiated the cooperative self-assembly of ordered mesophases and the condensation of silicates, as well as the deposition of copper oxide species. The copper oxide species in the resulting materials (abbreviated as CuMSN) were subsequently transformed to nanosized metallic copper by hydrogen reduction. We found that the reduced CuMSN exhibited superior catalytic activity and stability for the selective oxidation of propylene with O_2 to produce acrolein, and that the silanol groups on the silica surface of CuMSN facilitated the adsorption of propylene, thereby enhancing the conversion of the reactant. The acrolein yield for the best CuMSN was almost four times the value for the state-of-the-art SBA-15-supported copper catalyst under relatively mild reaction conditions [15]. Techniques including hydrogen temperature-programmed reduction, in situ X-ray absorption spectroscopy, and in situ diffuse reflectance infrared Fourier transform spectroscopy were employed to identify the promotional effect in the CuMSN-catalyzed oxidation of propylene by O_2.

2. Experimental

2.1. Materials preparation

The preparation of CuMSN was based on the "pH-jump" synthesis of pure silica MSNs [45]. The solution containing cetyltrimethylammonium bromide (1.14 g, Acros), sodium metasilicate (2.02 g, J.T. Baker), and water (675 mL) was mixed well with a calculated amount of the stock solution of the ammonia complex of Cu(II) (prepared by adding ammonia solution (50 mL, 3.0 M) into an aqueous solution (50 mL, 0.1 M) of copper nitrate (Showa)). EA (9.76 mL, Alfa) was then quickly added to the mixture, which was vigorously stirred for 30 s, then kept static at 35 °C for 24 h, and finally aged at 90 °C for 24 h. The surfactant molecules in the as-synthesized samples were removed by calcination at 540 °C or by repeated solvent extraction (with an ethanol solution of ammonium nitrate (0.025 M) at 50 °C for 15 min for three times). The calcined and solvent-extracted samples with varied copper-to-silicon (Cu/Si) ratios of *x*% are denoted as *x*CuMSN-C and *x*CuMSN-E, respectively.

A reference sample with Cu/Si of 3% was prepared by impregnation of the calcined pure silica material (i.e., 0CuMSN-C) with an aqueous solution of copper nitrate followed by calcination at 540 °C. The reference sample is denoted as 3CuMSN-IC.

2.2. Materials characterization

Dynamic light scattering (DLS) measurements were conducted on a particle size analyzer (Brookhaven Instruments Corporation, Holtsville, NY). Inductively coupled plasma–mass spectroscopy (ICP-MS) data were obtained using a Perkin–Elmer SCIEX-ELAN 5000 device. Powder X-ray diffraction (PXRD) patterns were obtained on a Mac Science 18MPX diffractometer using CuKα radiation. N_2 physisorption isotherms were measured at 77 K using a Quantachrome Autosorb-1-MP instrument. The desorption branches were analyzed by the density functional theory (DFT) method to evaluate pore sizes, and the adsorption branches in the relative pressure range 0.05–0.30 were used to calculate surface areas by the Brunauer–Emmett–Teller (BET) method. Pore volumes were evaluated at a relative pressure of 0.95. Solid-state ^{29}Si MAS NMR spectra were measured on a Bruker AVANCE III spectrometer using a 4-mm MAS probe. SEM images were obtained with a field emission JEOL JSM-7000F microscope operating at 10 kV and equipped with an energy dispersion X-ray (EDX) spectrometer. The samples were coated with Pt before measurements were performed. TEM images were taken using a JEOL JEM-2010 microscope operated at 200 kV and equipped with an EDX spectrometer. Diffuse reflectance UV–visible absorption spectra were recorded on a JASCO V-650 spectrophotometer equipped with a diffuse reflectance accessory.

2.3. Hydrogen temperature-programmed reduction

Hydrogen temperature-programmed reduction (H_2 TPR) was performed at atmospheric pressure in a conventional flow system. A sample (40 mg) was placed in a tubular reactor and heated at a rate of 10 °C min^{-1} in a mixed gas stream (10% H_2 and 90% N_2) with a flow rate of 30 mL min^{-1}. The *K*- and *P*-values for the measurements were 55–140 s and 5–20 K, respectively [46,47]. A cold trap that contained a gel formed by the addition of liquid nitrogen to acetone in a Thermos flask was used to prevent water from entering the thermal conductivity detector.

2.4. Estimation of surface area and dispersion of metallic copper

The surface area and the dispersion of metallic copper in the reduced CuMSN catalysts were estimated by a method combining H_2 TPR and N_2O oxidation [15,30]. The freshly prepared catalyst was first analyzed by H_2 TPR to calculate the total number of copper atoms in that catalyst. After H_2 TPR, the reduced catalyst was cooled to 80 °C under N_2, and the atmosphere was then switched to 10% N_2O/N_2 for 30 s to oxidize the surface atoms of the metallic copper nanoparticles to Cu (I) according to the reaction $2Cu_{(s)} + N_2O_{(g)} \rightarrow Cu_2O_{(s)} + N_{2(g)}$. The thus-produced Cu_2O monolayer was quantified by H_2 TPR and the amount of H_2 consumed was used to calculate the surface area of copper by assuming an average surface density for the metal of 1.4×10^{19} atoms m^{-2} [15,30]. The dispersion of copper was calculated from the number of surface copper atoms and the total copper content of the catalyst. The data were also used to estimate the average particle size of copper nanoparticles in the reduced catalyst by assuming a spherical particle shape. The equations to calculate surface area (S_{Cu}), dispersion (D_{Cu}), and average particle size (d_{Cu}) of copper nanoparticles are

$$S_{Cu}\,(\text{in m}^2/\text{g}_{Cu}) = (2 \times Y \times N_{av})/(X \times M_{Cu} \times 1.47 \times 10^{19}) \approx 1353 \times Y/X,$$

$$D_{Cu}\,(\text{in }\%) = (2 \times Y/X) \times 100\%,$$

$$d_{Cu}\,(\text{in nm}) = 6/(S \times \rho_{Cu}),$$

where *X* is the H_2 consumption for complete reduction of the copper in the catalyst, *Y* is the H_2 consumption for the reduction of surface Cu(I) species (formed by N_2O oxidation), N_{av} is Avogadro's constant (6.02×10^{23} mol^{-1}), M_{Cu} is the relative atomic mass of copper

(63.546 g mol^{-1}), and ρ_{Cu} is the density of metallic copper (8.92 g cm^{-3}).

2.5. In situ X-ray absorption spectroscopy measurements

Cu *K*-edge X-ray absorption spectroscopy (XAS) data were collected on the beamlines 17C at the National Synchrotron Radiation Research Center (NSRRC, Taiwan) with a storage ring energy of 1.5 GeV and an electron beam current of 360 mA in a top-up injection mode. The powdered catalyst was packed into a holder before being mounted in an in situ cell for transmission measurements. The X-ray absorption near-edge structure (XANES) and the extended X-ray absorption fine structure (EXAFS) were recorded after exposure to varied conditions (to mimic those for catalyst pretreatment and catalytic reactions) and cooling to room temperature in He to monitor the change of oxidation state and the coordination of copper species [15]. Multiple scans were averaged to improve the signal-to-noise ratio.

2.6. Catalytic studies

A fixed-bed flow reactor was used for the studies. Before the reaction, the catalyst (50 mg) was pretreated on line under a pure H_2 flow at 350 °C for 1 h and was then cooled to a designated reaction temperature (typically 180, 220, or 260 °C) under He. The reaction gas, consisting of 5% propylene and 5% O_2 in He with a flow rate of 25 mL min^{-1} (corresponding to a space velocity of 30,000 cm^3 h^{-1} g_{cat}^{-1}), was preheated before passing over the catalyst. The gas leaving the reactor was analyzed every 45 min by an Agilent 7890A gas chromatography system equipped with a Molsieve 5A and a Porabond Q column, each with a thermal conductivity detector and a flame ionization detector. The carbon balance was close to 100 ± 3%. The parameters of propylene conversion, acrolein selectivity, acrolein yield (Y_{AC}), acrolein formation rate (R_{AC}), and turnover frequency (TOF) are defined as follows:

Propylene conversion = moles of (oxygenates + CO_2/3)/moles of C_3H_6 in feed,
Acrolein selectivity = moles of acrolein/moles of (oxygenates + CO_2/3),
Y_{AC} = propylene conversion × acrolein selectivity,
R_{AC} = (Y_{AC} × flow rate × propylene concentration)/(molar volume of a gas at NTP × weight of copper),
TOF = (propylene conversion × flow rate × propylene concentration)/(molar volume of a gas at NTP × number of surface copper atoms).

The moles of surface copper atoms were derived from the surface area of copper and an average surface density for the metal of 1.46 × 10^{19} atoms m^{-2} [15,30].

2.7. In situ diffuse reflectance infrared Fourier transform spectroscopy measurements

The study was performed using a Thermo-Nicolet 6700 spectrometer equipped with a mercury cadmium telluride (MCT) detector. The instrument was operated at a 1 cm^{-1} resolution, and 256 scans were collected. A sample was mounted in a diffuse reflectance infrared Fourier transform spectroscopy (DRIFTS) cell (Harrick) equipped with ZnSe windows and a heating cartridge. The cell was heated to a designated temperature under a controlled atmosphere and was then purged with an He stream for 1 h to remove residual gases before measurements.

3. Results and discussion

The silica-supported copper materials were synthesized by applying the pH-jump method reported for MCM-41-type MSNs, with the ammonia complex of Cu(II) as a metal precursor [45]. The ammonia complex was stable under the alkaline conditions and the synthesis solution remained clear and showed no signal in DLS analysis before EA was added. After EA addition, the drastic drop of solution pH caused by the hydrolysis of EA destabilized the copper complex, triggered the polycondensation of silicate and copper species, and in the meantime initiated the cooperative assembly of an ordered organic–inorganic mesophase. All the copper species were precipitated out in the solid products, as confirmed by ICP-MS analysis of the filtrates of the synthesis solutions and EDX analysis of the solid products. The materials were composed of rather uniform nanoparticles with sizes of 100–200 nm (cf. Fig. S1 in the Supplementary Material for a typical SEM image of 3CuMSN). Since the solution pH eventually became nearly neutral, the degree of silica condensation for the samples was high, as evidenced by the relatively high intensity of the Q^4 line (Q^n: (Si(OSi)$_n$(OH)$_{4-n}$, n = 2, 3, 4) in the solid-state ^{29}Si MAS NMR spectra of the solvent-extracted samples (cf. Fig. S2 for the spectra of 3CuMSN-E and the calcined sample 3CuMSN-C). The fact that the Q^3 and Q^2 lines for 3CuMSN-E were more intense than those for 3CuMSN-C was associated with the presence of more silanol groups in the solvent-extracted sample. Although the total intensity ratios of Q^2 and Q^3 for 3CuMSN-C (28%) and for 3CuMSN-E (32%) did not differ very much, the difference is significant, especially for highly condensed silica materials such as 3CuMSN-E and 3CuMSN-C. It was noted that the process of solvent extraction did not result in leaching of copper from the samples, and the Cu/Si ratios for the calcined and solvent-extracted samples were nearly identical to the corresponding nominal values of the molar ratios of sodium metasilicate and the ammonia complex of Cu(II) in the synthesis solutions (as confirmed by ICP-MS). The copper in the extracted and calcined CuMSN samples formed oxide-like species, as suggested by the Cu *K*-edge XANES measurements. Fig. S3 shows the XANES spectra and their first derivatives for 3CuMSN-E, 3CuMSN-C, and reference materials. Obviously the spectra of the two samples resembled that of CuO with a shift of absorption edge toward higher energy. The observed energy shift may be correlated with the chemical environment of the copper species in the samples. The sample 3CuMSN-E was further subjected to a leaching test by stirring in an aqueous solution of hydrogen chloride (0.15 N) at 50 °C for 2 h, and about 67% of the copper survived the test. This suggested that most copper species were strongly bound to the silica framework, some of which might be resident and isolated in the silica framework, to exhibit such stability against acid leaching.

Supplementary data associated with this article can be found, in the online version, at https://doi.org/10.1016/j.jcat.2018.07.014.

As expected, similar textural properties of the calcined and solvent-extracted samples were observed (cf. Fig. 1 and Table S1). Small-angle PXRD patterns of *x*CuMSN-C indicated that the calcined samples with Cu/Si ratio up to 9% exhibited a well-ordered 2D-hexagonal mesostructure (cf. Fig. 1A), and further increase of the Cu/Si ratio resulted in materials with a lower degree of structural order. The absence of reflections in the wide-angle PXRD regime suggested that the oxide species of copper dispersed well in the materials (cf. Fig. S4). The *x*CuMSN-C samples showed type IV N_2 physisorption isotherms (cf. Fig. 1B) with steps at relative pressure (P/P_0) at 0.25–0.35, indicating the presence of ~3.4–3.7-nm-wide channel-type mesopores. The H2-type hysteresis loops at P/P_0 = 0.50–0.95 may be associated with the presence of extensive intraparticle voids, and a similar phenomenon was

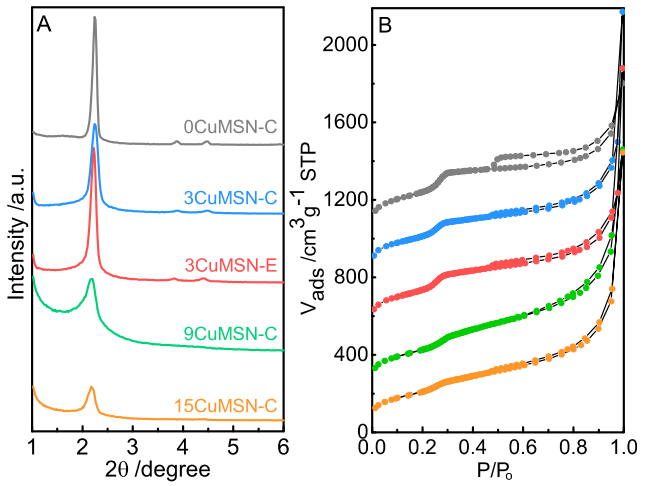

Fig. 1. Small-angle PXRD patterns (A) and N_2 physisorption isotherms (B) of selected CuMSN samples. The isotherms are shifted (from bottom to top) by 0, 200, 500, 800, and 1000 cm^3 g^{-1} STP, respectively.

observed for MSNs synthesized by the pH-jump method [45]. The samples exhibited high surface area and large pore volume, and the values decreased with increasing Cu/Si ratio, accompanied by a small increase in pore wall thickness (cf. Table S1). The results suggested that the mesopores in *x*CuMSN-C were fully open without being clogged by the copper species.

Fig. 2 shows TEM images of selected samples. For the pure-silica 0CuMSN-C, identical to the MCM-41 MSNs previously reported [45], the presence of extensive voids that may be beneficial for mass transport in catalytic processes was observed in each particle. When the ammonia complex of Cu(II) was introduced into the synthesis solution, the voids became slightly wider and more interconnected, while the 2D-hexagonal mesostructure was preserved (cf. Fig. 2B and 2C). This was also reflected in the changes of the shape of the hysteresis loop and the slope of the adsorption/desorption curves at P/P_0 = 0.50–0.95. No discernable domains composed solely of copper oxides were observed, even for 9CuMSN-C. For comparison, a reference sample, 3CuMSN-IC (with Cu/Si = 3%), was prepared by impregnation. PXRD and N_2 physisorption analyses indicated that 3CuMSN-IC contained CuO particles (JCPDS file 48–1548) that clogged the mesopores of the sample (cf. Fig. S5 and Table S1). In line with the data, some CuO nanoparticles near the pore openings could be observed by TEM (cf. Fig. 2D). Diffuse reflectance UV–visible spectra were further recorded to probe the coordination state of the copper species. As shown in Fig. S6, 3CuMSN-E and 3CuMSN-C showed a strong absorption peak at ca. 225 nm and a shoulder absorption between 275 and 350 nm, which could be assigned to the charge transfer transition between isolated Cu^{2+} with framework oxygen and $[Cu—O—Cu]_n$ cluster species, respectively [48]. On the other hand, 3CuMSN-IC exhibited noticeable broad absorption at about 400–800 nm, attributed to the d–d transition of Cu^{2+} in the octahedral ligand environment, indicating the presence of CuO particles [48]. In summary, the results showed the simplicity and uniqueness of the pH-jump method of preparing copper-containing mesoporous silica materials with highly dispersed metal species. The method may be applied to prepare the same type of materials containing other metals such as Ti, Cr, Mn, Co, Ni, and Zn using ammonia or suitable amine-type ligands. Detailed studies are in progress and will be reported elsewhere.

H_2 TPR and combined N_2O oxidation/H_2 TPR analyses were then conducted on the samples with Cu/Si = 3% to gain information about the dispersion of the metallic copper after hydrogen reduction. As shown in Fig. 3 (solid lines), 3CuMSN-C and 3CuMSN-E exhibited intensive and relatively sharp but slightly tailing H_2 TPR peaks at 235 and 255 °C, respectively, representing the reduction of small and finely dispersed copper oxide as well as isolated copper species [15,48–50]. On the other hand, 3CuMSN-IC started to take up hydrogen at ~110 °C and showed broad overlapping peaks at 226 and 260 °C, suggesting the presence of both relatively

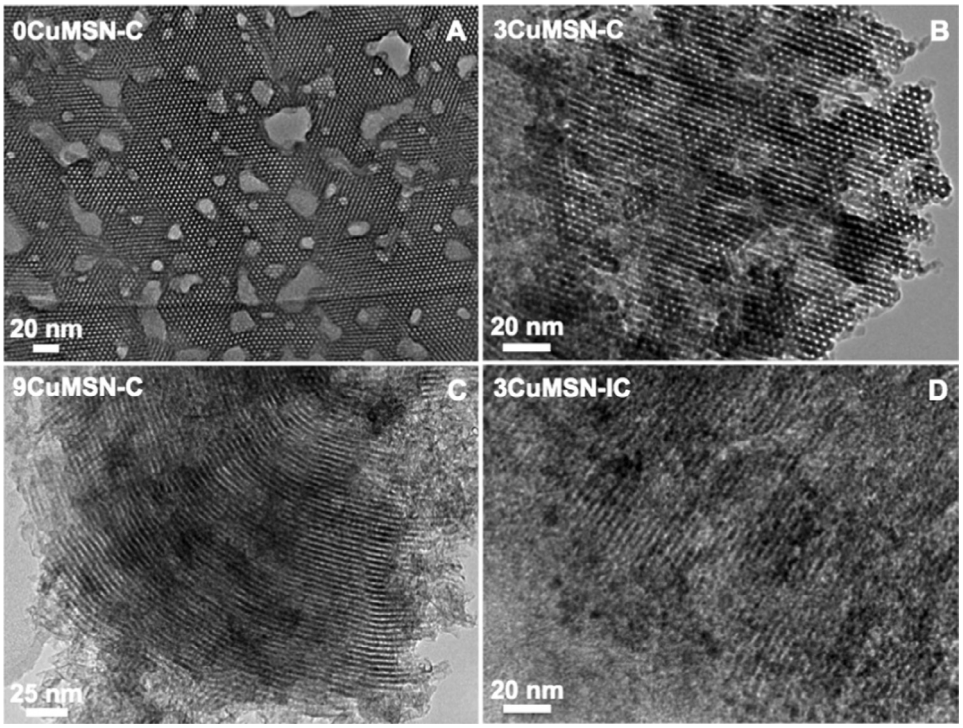

Fig. 2. TEM images of 0CuMSN-C (A), 3CuMSN-C (B), 9CuMSN-C (C), and 3CuMSN-IC (D).

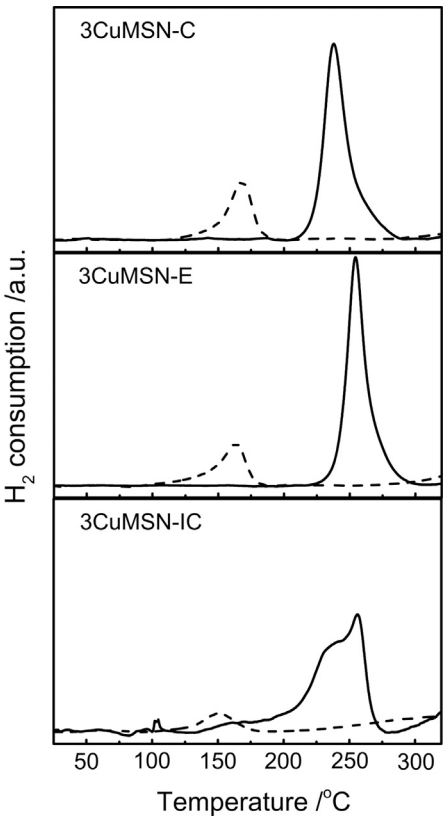

Fig. 3. H_2 TPR profiles of 3CuMSN-C, 3CuMSN-E, and 3CuMSN-IC. Solid and dashed lines are measured profiles of hydrogen consumption for the first and second TPR after N_2O oxidation, respectively.

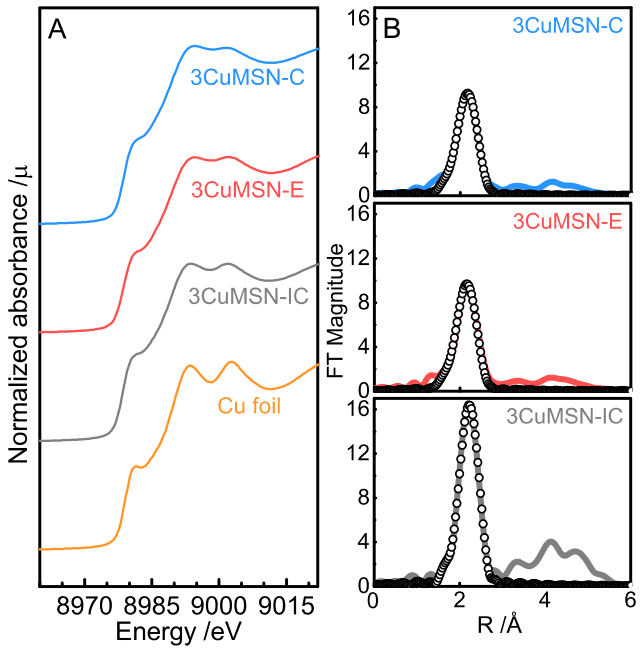

Fig. 4. (A) Cu *K*-edge XANES spectra of H_2-reduced 3CuMSN-E, 3CuMSNB-C, and 3CuMSN-IC. The spectrum of Cu foil is also shown for comparison. (B) FT profiles of Cu *K*-edge k^3-weighted EXAFS data (–) and the fitted results (o) of the three reduced samples.

nonuniform CuO and isolated copper species in this sample [48]. After the first H_2 TPR, the samples were subjected to N_2O oxidation of the surface copper atoms, followed by H_2 TPR. For the second H_2 TPR (cf. the dashed lines in Fig. 3), 3CuMSN-E and 3CuMSN-C exhibited major hydrogen uptake at ~165 °C, while a small and broad peak at ~150 °C was observed for 3CuMSN-IC. The amounts of hydrogen uptake in the temperature range of 100–350 °C were used to calculate the surface area of the metallic nanoparticles, from which the dispersion and particle size of copper were estimated. As shown in Table S2, the metal exhibited high dispersion (>50%) for both 3CuMSN-C and 3CuMSN-E, and the estimated particle sizes were ~1.6 and 2.0 nm, respectively. The copper dispersion for 3CuMSN-IC was relatively low (<10%), suggesting a larger particle size of the metal in this sample.

In addition to H_2 TPR, Cu K-edge XAS measurements were further conducted for particle size estimation. Each sample was reduced by hydrogen at 350 °C in an in situ cell prior to the measurements, and complete reduction of Cu was confirmed by XANES (cf. Fig. 4A). The data of EXAFS were further analyzed, and the Fourier transform (FT) profiles of the k^3-weighted EXAFS data and the curve-fitting results are shown in Fig. 4B and Table S2. The FT profiles of the three samples mainly consist of a first-shell peak corresponding to the nearest-neighbor Cu—Cu distance of 2.50–2.53 Å, which was reasonable for nanosized Cu particles [15]. The derived Cu—Cu coordination numbers (CNs) for 3CuMSN-C and 3CuMSN-E were significantly smaller than that for 3CuMSN-IC, and the estimated average sizes of Cu particles in the two one-pot synthesized samples were 0.9 and 1.3 nm, respectively, in comparison with that of 1.9 nm for 3CuMSN-IC. For the impregnated sample, the inconsistency between the particle sizes estimated from TPR and XAS (~10 and ~2.0 nm, respectively) might be due to possible sintering [51] of the nonuniform metallic copper particles during the first H_2 TPR to form relatively large and nonspherical particles in the mesopores of host silica. In summary, the results of UV–visible spectroscopy and TPR and XAS measurements indicated that the one-pot pH-jump synthesis resulted in materials with highly dispersed CuO clusters and isolated Cu^{2+} species that could be reduced to form very small metallic copper nanoparticles.

The H_2-reduced samples 3CuMSN-E, 3CuMSN-C, and 3CuMSN-IC were applied as catalysts for the oxidation of propylene by O_2 at 180–260 °C. Fig. 5 compares the changes in the conversion of propylene and the selectivities of acrolein and CO_2 with time on stream at 220 °C. Decreases in propylene conversion and CO_2 selectivity and an increase in acrolein selectivity were observed during the first 90 min of reaction for all the catalysts. Steady-state activities were reached within ~2 h and remained nearly unchanged even after further reaction for 12 h.

The high stability of the copper catalysts may be associated with the confinement effect of mesopores and relatively strong interaction between the nanosized copper and silica support. The initial decrease in propylene conversion for 3CuMSN-E and 3CuMSN-C (14–18%) was much smaller than that (~50%) for the impregnated sample 3CuMSN-IC. Table 1 summarizes the steady-state values of propylene conversion, O_2 conversion, products selectivity, acrolein yield, acrolein formation rate, and turnover frequency (TOF). The catalysts mainly produced acrolein and CO_2; ethanal and trace amounts of propylene oxide, propanal, acetone, ethylene, and methane were also detected. It was noted that while acrolein was the main product for these catalysts, some reported silica-supported copper catalysts mainly produced propylene oxide at temperatures below 250 °C. This may be attributed to the distinct structural and chemical properties of the copper species in the catalysts prepared by different routes, since these properties may affect the detailed mechanisms of the catalytic reactions. The conversion of propylene and O_2 increased, accompanied by the rise of acrolein yield (despite a slight drop in acrolein selectivity) as the reaction temperature was elevated from 180 to 260 °C.

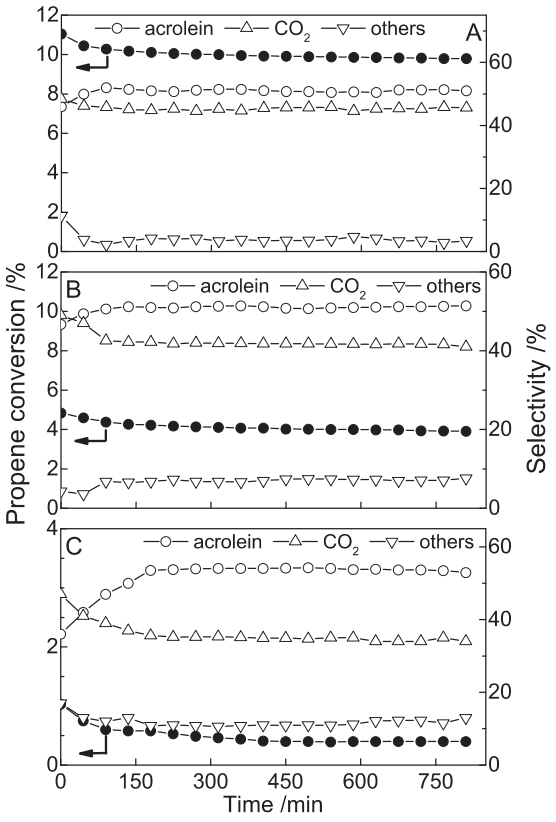

Fig. 5. Changes in propylene conversion (closed circles) and product selectivities (open symbols) with on-stream time at 220 °C for the H_2-reduced 3CuMSN-E (A), 3CuMSN-C (B), and 3CuMSN-IC (C).

Obviously, the catalytic activity of 3CuMSN-E and 3CuMSN-C was much better than that of 3CuMSN-IC, which may be attributed mainly to the small size and high dispersion of the metallic copper in the one-pot-synthesized catalysts. The acrolein yield for 3CuMSN-C at 260 °C was about an order of magnitude higher than that for 3CuMSN-IC. Moreover, 3CuMSN-E exhibited much higher catalytic activity than 3CuMSN-C in terms of the conversion of propylene and O_2 and the yield and formation rate of acrolein and TOF. As compared with the state-of-art SBA-15-supported copper catalyst (denoted as F-1-V with 1 wt.% copper loading in Ref. [15]) catalyzing the same reaction at 260 °C [15], 3CuMSN-E gave almost four times higher acrolein yield of 12.1% (cf. 3.2% for F-1-V) and a significantly higher acrolein formation rate of 236 $mmol_{acrolein}\ g_{Cu}^{-1}\ h^{-1}$ and TOF of 60.0 h^{-1} (cf. 196 $mmol_{acrolein}\ g_{Cu}^{-1}\ h^{-1}$ and 21.7 h^{-1} for F-1-V [15]). To provide a better comparison of the catalysts' selectivity, catalytic tests with varied catalyst weights (1.5–60 mg) and flow rates (3–25 mL min^{-1}) at 220 °C were performed to make a plot of acrolein selectivity versus propylene conversion (cf. Fig. S7), from which (combined with the results of H_2 TPR) the initial TOF (per surface copper atom) was calculated (cf. Table S3). The initial TOF for 3CuMSN-E was found to be around twice the value for 3CuMSN-C, which was significantly higher than that for3CuMSN-IC. A comparison of catalytic activity and reaction conditions for selected copper-based catalysts in the selective oxidation of propylene to acrolein is shown in Table S4.

The sample 3CuMSN-E was further analyzed to unveil factors contributing to its superior catalytic performance. Since the product selectivity of copper catalysts for the selective oxidation of propylene with O_2 is known to be strongly associated with the oxidation state of the metal [1,11,17,19,20,41], in situ XANES measurements were employed to follow the change in oxidation state of the copper species in the H_2-reduced 3CuMSN-E after exposure to the reaction mixture at different temperatures. All the spectra were acquired after the sample was exposed to different conditions for 2 h to ensure that the steady state was reached. As shown in Fig. 6, the first maximum of the first derivative shifted from 8978.8 to 8979.9 eV right after the H_2-reduced sample was exposed to the O_2-containing mixture at room temperature, indicating that the exposure resulted in immediate oxidation of a significant fraction of surface metallic copper to Cu^{1+} in 3CuMSN-E. A similar change was observed for the SBA-15-supported copper sample prepared by the same impregnation procedure as 3CuMSN-IC [15], but the fraction of copper being oxidized to Cu^{1+} was larger for 3CuMSN-E (mainly on the surfaces of metallic nanoparticles), as evidenced by the more pronounced shift of the first maximum of the first derivative. The Cu^{1+} cations that were in direct contact to the silica support may form Cu—O—Si bonds. Copper remained predominantly in the 1+ oxidation state after the sample was further heated to 260 °C under the same atmosphere. The results suggested that Cu^{1+} should be the active form in all the samples studied for the selective oxidation of propylene to produce acrolein as a major product, and the correlation of the oxidation state of copper and the product selectivity is consistent with previous studies on other types of copper catalysts [18,52,53].

On the other hand, the reduced 3CuMSN-E exhibited similar (slightly lower) copper dispersion yet much higher propylene conversion than the reduced 3CuMSN-C did. This pointed to the presence of some other factors that also contributed to the catalytic performance of 3CuMSN-E. Since the major difference between 3CuMSN-E and 3CuMSN-C was the number of silanol groups on

Table 1
Steady-state catalytic performance of selected H_2-reduced catalysts.[a]

Catalyst	T	Conversion %		Selectivity %				Y_{AC}	R_{AC}	TOF	E_a
	°C	O_2	C_3H_6	Acrolein	CO_2	Ethanal	Others	%	$mmol_{acrolein}\ g_{Cu}^{-1}\ h^{-1}$	h^{-1}	KJ mol^{-1}
3CuMSN-C	180	1.6	0.7	58	31	8	3	0.4	8	1.4	74
	220	9.4	3.9	51	42	6	1	2.0	39	7.7	
	260	33.9	13.9	50	41	4	5	6.9	136	27.3	
3CuMSN-E	180	3.4	1.7	56	37	6	1	1.0	19	4.1	67
	220	26.0	9.8	51	45	3	1	5.0	98	23.4	
	260	64.5	25.1	48	42	3	7	12.1	236	60.0	
3CuMSN-IC	180	0.2	0.1	59	29	8	4	0.1	1	1.0	74
	220	0.7	0.4	54	35	8	3	0.2	4	5.0	
	260	3.2	1.6	46	43	6	5	0.7	14	19.0	
3CuMSN-EM	180	1.1	0.5	63	26	8	3	0.3	6	0.2	57
	220	3.2	1.9	69	22	7	2	1.3	25	0.7	
	260	7.8	5.2	70	17	6	7	3.6	69	1.9	

[a] Y_{AC}: acrolein yield; R_{AC}: acrolein formation rate; TOF: turnover frequency; E_a: activation energy.

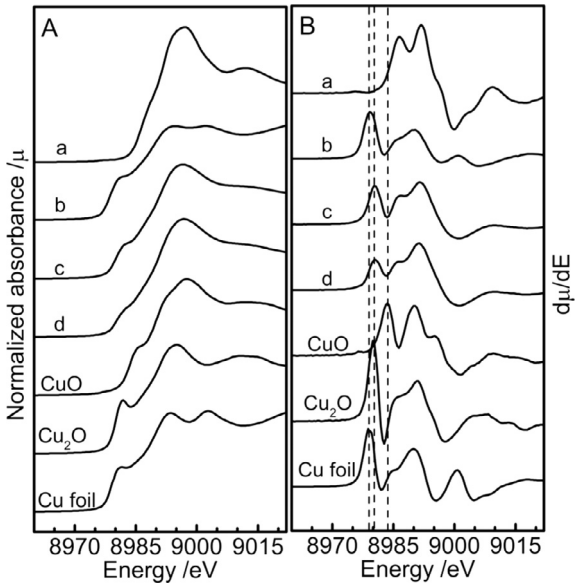

Fig. 6. Cu *K*-edge XANES spectra (A) and first-derivative XANES spectra (B) of the as-prepared 3-CuMSN-E (a) and the sample after reduction under H_2 at 350 °C (b), cooling down to 25 °C and exposure to the reaction mixture of propylene (5%), O_2 (5%), and He (90%) (c), and finally heating to 260 °C under the same atmosphere (d). The spectra of reference samples of CuO, Cu_2O, and Cu foil are also shown. The dashed lines in (B) indicate the positions of the first maxima for Cu foil (8978.8 eV), Cu_2O (8979.9 eV), and CuO (8983.5 eV).

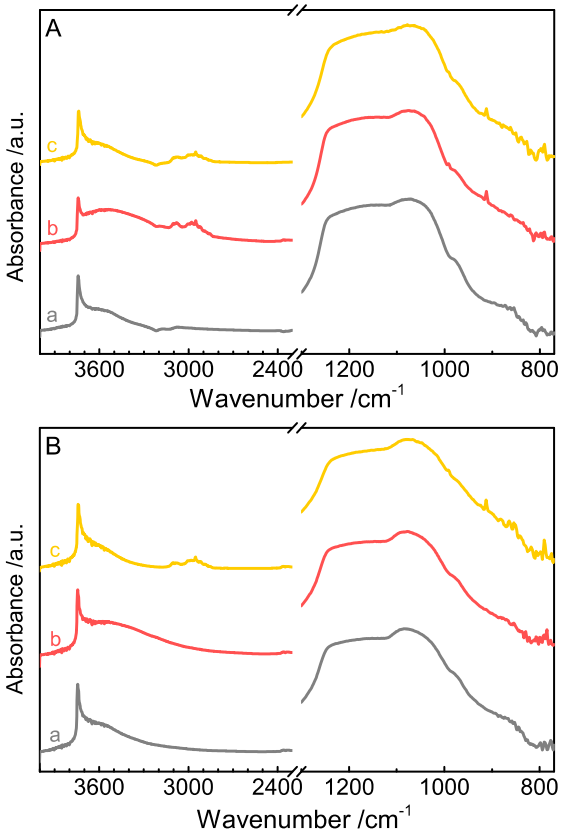

Fig. 7. In situ DRIFTS results of 3-CuMSN-E (A) and 3-CuMSN-C (B) after H_2 reduction (a), cooling down to 25 °C and exposure to the reaction mixture of propylene (5%), O_2 (5%), and He (90%) at 25 °C for 45 min followed by He purge (b), and finally heating to 260 °C and again exposure to the reaction mixture for 45 min followed by He purge (c).

the silica support (cf. Fig. S2), it was speculated that the surface silanol groups might become involved in the overall catalytic process. To examine this, 3CuMSN-E was reacted with hexamethyldisilazane (HMDS, Showa) to passivate the surface silanol groups via silylation. The reaction was confirmed by solid-state ^{29}Si MAS NMR, and the spectrum of the resulting sample (designated as 3CuMSN-EM) contained a new line attributed to the trimethylsilyl group (M line), weaker Q^2 and Q^3 lines, and a stronger Q^4 line as compared with the spectrum of 3CuMSN-E (cf. Fig. S8). The sample was reduced by the same process and the dispersion and particle size of the metallic copper in the reduced 3CuMSN-EM were nearly identical to those in the reduced 3CuMSN-E, as evidenced by H_2 TPR and N_2O oxidation/H_2 TPR (cf. Fig. S9). The reduced 3CuMSN-EM was applied to catalyze the reaction of propylene and O_2 under identical conditions, and the steady-state catalytic performance (reached within 2 h) is also shown in Table 1. Compared with the values for 3CuMSN-E, the conversion of propylene and O_2 for 3CuMSN-EM was much smaller, yet the acrolein selectivity was higher and relatively insensitive to reaction temperature. The high acrolein selectivity seems to correlate well with the low apparent activation energy for the passivated catalyst (cf. Table 1), which implies that the relative energy of the transition state for the reaction pathway leading to the formation of acrolein for 3CuMSN-EM might be lower than that for 3CuMSN-E.

The fact that much lower propylene conversion was observed for the surface-passivated 3CuMSN-EM suggested a possible role of the surface silanols in the adsorption of the reactant. In situ DRIFTS measurements on 3CuMSN-E and 3CuMSN-C were further conducted, and the results are shown in Fig. 7. A peak at 3740 cm^{-1} attributed to the isolated silanol groups and a band centered at 3400 cm^{-1} associated with the hydrogen-bonded silanol nests [54] were observed for both the H_2-reduced samples. It was noted that while the signal of isolated silanol groups is stronger for 3CuMSN-C, the band attributed to the silanol nests is more intense for 3CuMSN-E. After being exposed to the reaction gas mixture at room temperature, followed by an He purge to remove unadsorbed molecules, interestingly, only 3CuMSN-E exhibited a spectrum containing new peaks at 3100, 2954, 1442, 1477, and 912 cm^{-1}, which could be assigned to the vibrational modes of propylene [55,56]. This indicated that the surface silanols in 3CuMSN-E, probably those adjacent to the Cu^{1+} species immediately formed upon exposure to the reaction mixture, jointly and greatly promoted the adsorption of propylene and thereby facilitated the overall catalytic reaction. The silanol groups at the periphery of copper nanoparticles might also become involved in the oxidation of copper during catalytic reaction.

It was noted that peaks roughly at the same positions were observed for both samples after exposure to the reaction mixture at 260 °C followed by a He purge. The peaks might be attributed to the unreacted adsorbed propylene or some intermediates of the catalytic reaction on the catalysts. When all the results were combined, it could be concluded that the superior catalytic activity of 3CuMSN-E for the selective oxidation of propylene with O_2 to acrolein was mainly attributable to the small size of the metallic copper nanoparticles, which resulted in the oxidation of a large fraction of Cu^0 to Cu^{1+} upon exposure to the reaction mixture, and to the presence of surface silanols facilitating the adsorption of propylene on the copper catalyst and thereby enhancing the overall reaction rate.

4. Conclusions

A direct synthesis of mesoporous-silica-nanoparticle-supported nanosized copper catalysts has been reported. The catalysts feature ordered mesostructures with extensive voids, high surface area and large pore volume, high degree of silica condensation, and high

dispersion of copper species, which are strongly bound to the silica framework. The ionic copper species transform to highly dispersed and nanosized metallic copper after hydrogen reduction, and the reduced catalysts exhibit superior activity for the selective oxidation of propylene with dioxygen. The conversion of both reactants and the yield and formation rate of acrolein are high and stable. The excellent catalytic performance may be attributed mainly to the small size of metallic copper in the one-pot synthesized catalysts, which transforms to Cu^{1+} under reaction conditions, and the surface silanol groups contributed to propylene adsorption and facilitated the overall reaction.

Acknowledgments

The authors acknowledge Dr. Jyh-Fu Lee for help with the XAS measurements. The authors gratefully acknowledge the financial support of the Ministry of Science and Technology, Taiwan, under Contracts MOST 106-2113-M-007-025-MY3 and MOST 107-3017-F-007-002. This study was also supported by the Frontier Research Center on Fundamental and Applied Sciences of Matter from The Featured Areas Research Center Program within the framework of the Higher Education Sprout Project by the Ministry of Education (MOE) in Taiwan.

References

[1] M.B. Gawande, A. Goswami, F.-X. Felpin, T. Asefa, X. Huang, R. Silva, X. Zou, R. Zboril, R.S. Varma, Cu and Cu-based nanoparticles: synthesis and applications in catalysis, Chem. Rev. 116 (2016) 3722–3811.
[2] M. Behrens, Coprecipitation: an excellent tool for the synthesis of supported metal catalysts - from the understanding of the well known recipes to new materials, Catal. Today 246 (2015) 46–54.
[3] M. Yang, S. Li, Y. Wang, J.A. Herron, Y. Xu, L.F. Allard, S. Lee, J. Huang, M. Mavrikakis, M. Flytzani-Stephanopoulos, Catalytically active Au-O(OH)x-species stabilized by alkali ions on zeolites and mesoporous oxides, Science 346 (2014) 1498–1501.
[4] F. Schüth, M. Hesse, K.K. Unger, Precipitation and Coprecipitation, in: Handbook of Heterogeneous Catalysis, Wiley-VCH, 2008.
[5] S. Sato, R. Takahashi, T. Sodesawa, K.-I. Yuma, Y. Obata, Distinction between surface and bulk oxidation of Cu through N_2O decomposition, J. Catal. 196 (2000) 195–199.
[6] R. van den Berg, C.F. Elkjaer, C.J. Gommes, I. Chorkendorff, J. Sehested, P.E. de Jongh, K.P. de Jong, S. Helveg, Revealing the formation of copper nanoparticles from a homogeneous solid precursor by electron microscopy, J. Am. Chem. Soc. 138 (2016) 3433–3442.
[7] D. Wang, D. Astruc, The recent development of efficient earth-abundant transition-metal nanocatalysts, Chem. Soc. Rev. 46 (2017) 816–854.
[8] P. Liu, R. Qin, G. Fu, N. Zheng, Surface coordination chemistry of metal nanomaterials, J. Am. Chem. Soc. 139 (2017) 2122–2131.
[9] H. Shimizu, I. Nagasaki, K. Matsumura, N. Sayo, T. Saito, Developments in asymmetric hydrogenation from an industrial perspective, Acc. Chem. Res. 40 (2007) 1385–1393.
[10] D. Ma, Q. Cai, Copper/amino acid catalyzed cross-couplings of aryl and vinyl halides with nucleophiles, Acc. Chem. Res. 41 (2008) 1450–1460.
[11] W. Song, D.M. Perez Ferrandez, L. van Haandel, P. Liu, T.A. Nijhuis, E.J.M. Hensen, Selective propylene oxidation to acrolein by gold dispersed on $MgCuCr_2O_4$ spinel, ACS Catal. 5 (2015) 1100–1111.
[12] G. Li, P. Vassilev, M. Sanchez-Sanchez, J.A. Lercher, E.J.M. Hensen, E.A. Pidko, Stability and reactivity of copper oxo-clusters in ZSM-5 zeolite for selective methane oxidation to methanol, J. Catal. 338 (2016) 305–312.
[13] R.V. Goncalves, R. Wojcieszak, H. Wender, C. Sato, B. Dias, L.L.R. Vono, D. Eberhardt, S.R. Teixeira, L.M. Rossi, Easy access to metallic copper nanoparticles with high activity and stability for CO oxidation, ACS Appl. Mater. Interf. 7 (2015) 7987–7994.
[14] S.S. Acharyya, S. Ghosh, S. Adak, D. Tripathi, R. Bal, Fabrication of $CuCr_2O_4$ spinel nanoparticles: a potential catalyst for the selective oxidation of cycloalkanes via activation of C_{sp3}–H bond, Catal. Commun. 59 (2015) 145–150.
[15] C.-H. Liu, N.-C. Lai, J.-F. Lee, C.-S. Chen, C.-M. Yang, SBA-15-supported highly dispersed copper catalysts: vacuum-thermal preparation and catalytic studies in propylene partial oxidation to acrolein, J. Catal. 316 (2014) 231–239.
[16] S.D. Senanayake, D. Stacchiola, J.A. Rodriguez, Unique properties of ceria nanoparticles supported on metals: novel inverse ceria/copper catalysts for CO oxidation and the water-gas shift reaction, Acc. Chem. Res. 46 (2013) 1702–1711.
[17] S. Belin, C.L. Bracey, V. Briois, P.R. Ellis, G.J. Hutchings, T.I. Hyde, G. Sankar, $CuAu/SiO_2$ catalysts for the selective oxidation of propene to acrolein: the impact of catalyst preparation variables on material structure and catalytic performance, Catal. Sci. Technol. 3 (2013) 2944–2957.
[18] D. Duzenli, E. Seker, S. Senkan, I. Onal, Epoxidation of propene by high-throughput screening method over combinatorially prepared Cu catalysts supported on high and low surface area silica, Catal. Lett. 142 (2012) 1234–1243.
[19] C.L. Bracey, A.F. Carley, J.K. Edwards, P.R. Ellis, G.J. Hutchings, Understanding the effect of thermal treatments on the structure of $CuAu/SiO_2$ catalysts and their performance in propene oxidation, Catal. Sci. Technol. 1 (2011) 76–85.
[20] H. Tüysüz, J. Galilea, F. Schüth, Highly diluted copper in a silica matrix as active catalyst for propylene oxidation to acrolein, Catal. Lett. 131 (2009) 49–53.
[21] W. Su, S. Wang, P. Ying, Z. Feng, C. Li, A molecular insight into propylene epoxidation on Cu/SiO_2 catalysts using O_2 as oxidant, J. Catal. 268 (2009) 165–174.
[22] Q. Hu, G. Fan, L. Yang, F. Li, Aluminum-doped zirconia-supported copper nanocatalysts: surface synergistic catalytic effects in the gas-phase hydrogenation of esters, ChemCatChem 6 (2014) 3501–3510.
[23] A. Dhakshinamoorthy, S. Navalon, D. Sempere, M. Alvaro, H. Garcia, Reduction of alkenes catalyzed by copper nanoparticles supported on diamond nanoparticles, Chem. Commun. 49 (2013) 2359–2361.
[24] A. Ungureanu, B. Dragoi, A. Chirieac, S. Royer, D. Duprez, E. Dumitriu, Synthesis of highly thermostable copper-nickel nanoparticles confined in the channels of ordered mesoporous SBA-15 silica, J. Mater. Chem. 21 (2011) 12529–12541.
[25] P. Munnik, M. Wolters, A. Gabrielsson, S.D. Pollington, G. Headdock, J.H. Bitter, P.E. de Jongh, K.P. de Jong, Copper nitrate redispersion to arrive at highly active silica-supported copper catalysts, J. Phys. Chem. C 115 (2011) 14698–14706.
[26] G. Yin, M. Nishikawa, Y. Nosaka, N. Srinivasan, D. Atarashi, E. Sakai, M. Miyauchi, Photocatalytic carbon dioxide reduction by copper oxide nanocluster-grafted niobate nanosheets, ACS Nano 9 (2015) 2111–2119.
[27] S. Paria, O. Reiser, Copper in photocatalysis, ChemCatChem 6 (2014) 2477–2483.
[28] L. De Rogatis, M. Cargnello, V. Gombac, B. Lorenzut, T. Montini, P. Fornasiero, Embedded phases: a way to active and stable catalysts, ChemSusChem 3 (2010) 24–42.
[29] H.W. Slamet, E. Nasution, S. Purnama, J. Kosela, Gunlazuardi, photocatalytic reduction of CO_2 on copper-doped titania catalysts prepared by improved-impregnation method, Catal. Commun. 6 (2005) 313–319.
[30] Z.-Q. Wang, Z.-N. Xu, S.-Y. Peng, M.-J. Zhang, G. Lu, Q.-S. Chen, Y. Chen, G.-C. Guo, High-performance and long-lived Cu/SiO_2 nanocatalyst for CO_2 hydrogenation, ACS Catal. 5 (2015) 4255–4259.
[31] L. Mo, E.T. Saw, Y. Du, A. Borgna, M.L. Ang, Y. Kathiraser, Z. Li, W. Thitsartarn, M. Lin, S. Kawi, Highly dispersed supported metal catalysts prepared via *in-situ* self-assembled core-shell precursor route, Int. J. Hydrogen Energy 40 (2015) 13388–13398.
[32] L. Mo, S. Kawi, An *in situ* self-assembled core–shell precursor route to prepare ultrasmall copper nanoparticles on silica catalysts, J. Mater. Chem. A 2 (2014) 7837–7844.
[33] P. Gaudin, S. Dorge, H. Nouali, M. Vierling, E. Fiani, M. Moliere, J.-F. Brilhac, J. Patarin, CuO/SBA-15 materials synthesized by solid state grinding: influence of CuO dispersion and multicycle operation on $DeSO_X$ performances, Appl. Catal. B 181 (2016) 379–388.
[34] Y. Yin, W.-J. Jiang, X.-Q. Liu, Y.-H. Li, L.-B. Sun, Dispersion of copper species in a confined space and their application in thiophene capture, J. Mater. Chem. 22 (2012) 18514–18521.
[35] T. Yousefi Amiri, J. Moghaddas, Cogeled copper-silica aerogel as a catalyst in hydrogen production from methanol steam reforming, Int. J. Hydrogen Energy 40 (2015) 1472–1480.
[36] C.R. Adams, T.J. Jennings, Investigation of the mechanism of catalytic oxidation of propylene to acrolein and acrylonitrile, J. Catal. 2 (1963) 63–68.
[37] A. Marimuthu, J. Zhang, S. Linic, Tuning selectivity in propylene epoxidation by plasmon mediated photo-switching of Cu oxidation state, Science 339 (2013) 1590–1593.
[38] Z. Zhai, A.B. Getsoian, A.T. Bell, The kinetics of selective oxidation of propene on bismuth vanadium molybdenum oxide catalysts, J. Catal. 308 (2013) 25–36.
[39] J. Huang, M. Haruta, Gas-phase propene epoxidation over coinage metal catalysts, Res. Chem. Intermed. 38 (2012) 1–24.
[40] T.A. Nijhuis, M. Makkee, J.A. Moulijn, B.M. Weckhuysen, The production of propene oxide: catalytic processes and recent developments, Ind. Eng. Chem. Res. 45 (2006) 3447–3459.
[41] J.S. Yu, L. Kevan, Catalytic partial oxidation of propylene to acrolein over copper(II)-exchanged M-X and M-Y zeolites where M = Mg^{2+}, Ca^{2+}, Li^+, Na^+, K^+, and H^+: evidence for separate pathways for partial and complete oxidation, J. Phys. Chem. 95 (1991) 3262–3271.
[42] F. Schüth, W. Schmidt, Microporous and mesoporous materials, Adv. Mater. 14 (2002) 629–638.
[43] K.L. Boyesen, T. Kristiansen, K. Mathisen, Dynamic redox properties of vanadium and copper in microporous supports during the selective oxidation of propene, Catal. Today 254 (2015) 21–28.
[44] A. Fukuoka, J.-I. Kimura, T. Oshio, Y. Sakamoto, M. Ichikawa, Preferential oxidation of carbon monoxide catalyzed by platinum nanoparticles in mesoporous silica, J. Am. Chem. Soc. 129 (2007) 10120–10125.
[45] N.-C. Lai, C.-J. Lin, W.-C. Huang, C.-M. Yang, "pH-jump" synthesis of 2D-rectangular *c2mm* mesoporous silica materials with helical morphology and extensive void defects, Micropor. Mesopor. Mater. 190 (2014) 67–73.
[46] D.A.M. Monti, A. Baiker, Temperature-programmed reduction. Parametric sensitivity and estimation of kinetic parameters, J. Catal. 83 (1983) 323–335.

[47] P. Malet, A. Caballero, The selection of experimental conditions in temperature-programmed reduction experiments, J. Chem. Soc. Faraday Trans. 1 (84) (1988) 2369–2375.
[48] G. Zhang, J. Long, X. Wang, Z. Zhang, W. Dai, P. Liu, Z. Li, L. Wu, X. Fu, Catalytic role of Cu sites of Cu/MCM-41 in phenol hydroxylation, Langmuir 26 (2010) 1362–1371.
[49] B. Dragoi, A. Ungureanu, A. Chirieac, C. Ciotonea, C. Rudolf, S. Royer, E. Dumitriu, Structural and catalytic properties of mono- and bimetallic nickel–copper nanoparticles derived from MgNi(Cu)Al-LDHs under reductive conditions, Appl. Catal. A 504 (2015) 92–102.
[50] C. Tang, J. Sun, X. Yao, Y. Cao, L. Liu, C. Ge, F. Gao, L. Dong, Efficient fabrication of active CuO-CeO_2/SBA-15 catalysts for preferential oxidation of CO by solid state impregnation, Appl. Catal. B 146 (2014) 201–212.
[51] G. Agostini, R. Pellegrini, G. Leofanti, L. Bertinetti, S. Bertarione, E. Groppo, A. Zecchina, C. Lamberti, Determination of the particle size, available surface area, and nature of exposed sites for silica–alumina-supported Pd nanoparticles: a multitechnical approach, J. Phys. Chem. C 113 (2009) 10485–10492.
[52] J.B. Reitz, E.I. Solomon, Propylene oxidation on copper oxide surfaces: electronic and geometric contributions to reactivity and selectivity, J. Am. Chem. Soc. 120 (1998) 11467–11478.
[53] H. Chu, L. Yang, Q. Zhang, Y. Wang, Copper-catalyzed propylene epoxidation by molecular oxygen: superior catalytic performances of halogen-free K^+-modified CuO_x/SBA-15, J. Catal. 241 (2006) 225–228.
[54] A. Chang, H.-M. Hsiao, T.-H. Chen, M.-W. Chu, C.-M. Yang, Hierarchical silicalite-1 octahedra comprising highly-branched orthogonally-stacked nanoplates as efficient catalysts for vapor-phase Beckmann rearrangement, Chem. Commun. 52 (2016) 11939–11942.
[55] P. Concepcion, P. Botella, J.M.L. Nieto, Catalytic and FT-IR study on the reaction pathway for oxidation of propane and propylene on V- or Mo–V-based catalysts, Appl. Catal. A 278 (2004) 45–56.
[56] C. Zhao, I.E. Wachs, Selective oxidation of propylene to acrolein over supported V_2O_5/Nb_2O_5 catalysts: an *in situ* Raman, IR, TPSR and kinetic study, Catal. Today 118 (2006) 332–343.